

Accepted Manuscript

Synthesis, growth, physicochemical properties and DFT calculations of 2-naphthol substituted Mannich base 1-(morpholino(phenyl) methyl) naphthalen-2-ol: A non linear optical single crystal

A. Dennis Raj, M. Jeeva, M. Shankar, G. Venkatesa Prabhu, M. Vimalan, I. Vetha Potheher

PII: S0022-2860(17)30914-6

DOI: [10.1016/j.molstruc.2017.06.133](https://doi.org/10.1016/j.molstruc.2017.06.133)

Reference: MOLSTR 24019

To appear in: *Journal of Molecular Structure*

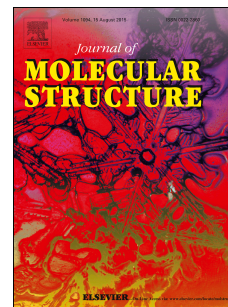
Received Date: 6 January 2017

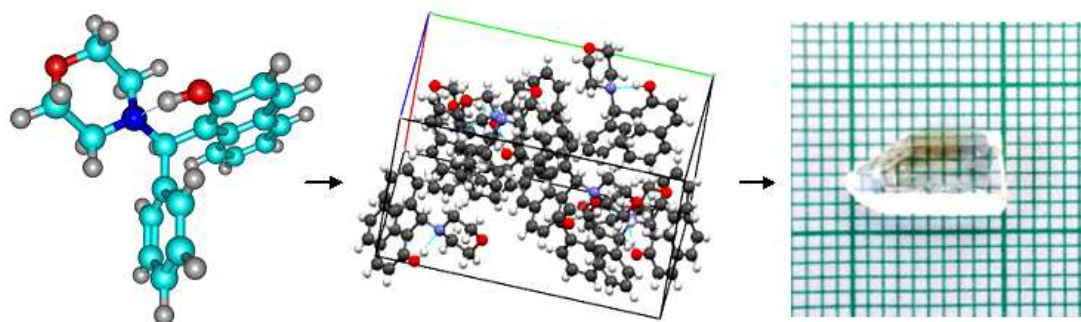
Revised Date: 29 June 2017

Accepted Date: 30 June 2017

Please cite this article as: A. Dennis Raj, M. Jeeva, M. Shankar, G. Venkatesa Prabhu, M. Vimalan, I. Vetha Potheher, Synthesis, growth, physicochemical properties and DFT calculations of 2-naphthol substituted Mannich base 1-(morpholino(phenyl) methyl) naphthalen-2-ol: A non linear optical single crystal, *Journal of Molecular Structure* (2017), doi: 10.1016/j.molstruc.2017.06.133.

This is a PDF file of an unedited manuscript that has been accepted for publication. As a service to our customers we are providing this early version of the manuscript. The manuscript will undergo copyediting, typesetting, and review of the resulting proof before it is published in its final form. Please note that during the production process errors may be discovered which could affect the content, and all legal disclaimers that apply to the journal pertain.





ACCEPTED MANUSCRIPT

Synthesis, Growth, Physicochemical properties and DFT calculations of 2-naphthol substituted Mannich base 1-(morpholino(phenyl) methyl) naphthalen-2-ol:

A Non linear Optical Single crystal

**A. Dennis Raj^a, M. Jeeva^b, M. Shankar^c, G. Venkatesa Prabhu^b, M. Vimalan^d,
I. Vetha Potheher^{c*}**

^aDepartment of Physics, Mookambigai College of Engineering, Pudukkottai - 622502, India.

^bDepartment of Chemistry, National Institute of Technology, Tiruchirappalli-620015, India.

^cDepartment of Physics, University College of Engineering, Bharathidasan Institute of Technology Campus, Anna University, Tiruchirappalli-620 024, India.

^dDepartment of Physics, Thirumalai Engineering College, Kilambi, Kancheepuram-631531, India.

Abstract

2-Naphthol substituted Mannich base 1-morpholino(phenyl)methyl)naphthalen-2-ol (MPMN), a potential NLO active organic single crystal was developed using acetonitrile as a solvent by slow evaporation method. The experimental and theoretical analysis made towards the exploitation in the field of electro-optic and NLO applications. The cubic structure with non-centrosymmetric space group Cc was confirmed and cell dimensions of the grown crystal were obtained from single crystal X-ray diffraction (XRD) study. The formation of the C-N-C vibrational band at 1115 cm⁻¹ in Fourier Transform Infra-Red (FTIR) analysis confirms the formation of MPMN compound. The placement of protons and carbons of MPMN were identified from Nuclear Magnetic Resonance Spectroscopy (NMR) analysis. The wide optical absorption window and the lower cutoff wavelength of MPMN show the suitability of the material for the various laser related applications. The presence of dislocations and growth pattern of crystal were analyzed using chemical etching technique. The second harmonic generation (SHG) of MPMN was found to be 1.57 times greater than the standard KDP crystal. The laser damage threshold was measured by using Nd: YAG laser beam through the sample and

it was found to be 1.006 GW/cm². The electronic structure of the molecular system and the optical properties were also studied from quantum chemical calculations using Density Functional Theory (DFT) and reported for the first time.

Keywords: Mannich Base, Molecular structure, Single crystal XRD, Density Functional Theory, Laser damage threshold.

***Corresponding Author:** Dr. I. Vetha Potheher, Assistant Professor of Physics, University College of Engineering, Bharathidasan Institute of Technology Campus, Anna University, Tiruchirappalli- 620024, India. Mobile: +919942994274, Email: potheher11@gmail.com

1. Introduction

In the recent years, Non-Linear Optical (NLO) crystals have attracted the researchers due to their potential applications in high power laser for inertial confinement fusion research [1, 2], electro-optic switches, frequency conversion [3], color display and photonics including optical information processing [4-7]. To have strong second-order NLO properties, the compound must possess a large first-order molecular hyper polarizability (β), and also must crystallize in a noncentro symmetric structure to have nonzero second-order polarizability (χ^2) [8]. It has been generally understood that, for a material to have useful and high efficient NLO properties, the constituting molecules must possess large molecular hyper polarizabilities, which are normally characterized by a highly extended π -conjugated electron donor–acceptor pairs at the ends [9]. Apart from the high nonlinear optical response, the NLO materials must also satisfy few other technological needs for practical applications such as wide optical transparency extending down to UV region, thermal stability, chemical stability and mechanical stability [8]. Comparing to inorganic materials, organic compounds are efficient materials to exhibit high NLO response which may be due to the presence of conjugated π electrons along with weak van der Waals interactions between the hydrogen bonds and available. These parameters are quite essential for most of their NLO properties [10]. The analyzes towards the device fabrication, organic NLO crystals are better than inorganic crystals due to their high conversion efficiency for second and higher order harmonic generation, good transparency in the visible region and high resistance offering for laser damage. Because of these properties, the organic materials can be applicable to many devices particularly optical storage devices and optical telecommunications. In addition, existing molecular flexibility is an added advantage to increase the nonlinearity of organic crystal in a desired manner [11, 12].

In recent trends, Mannich bases give much attention for the synthesis of various potential agents of high medicinal values like anti-inflammatory, anticancer, antibacterial, antifungal, anticonvulsant and various bio active molecular applications [13-16]. They also find a wide variety of commercial applications such as detergent additives, resins, polymers, surface active agents and corrosion inhibitors [17, 18]. Mannich reaction is a three component reaction in which a nonenolizable aldehyde, i.e. formaldehyde, a primary or secondary amine and an enolizable carbonyl compound react and give the end products known as Mannich bases. This reaction was developed by the Italian chemist Mario Betti in which the enolizable carbonyl compound is replaced by a molecule of β -naphthol or phenol. This is a useful method to synthesize aminoalkyl phenols or naphthols based compounds [19, 20]. Mannich bases possess short intramolecular hydrogen bond interaction between the hydroxyl group and the nitrogen of amine group which increases the NLO activity of the product molecule.

In order to search the theoretical and experimental uniformity, quantum chemical calculations were carried out with complete geometry optimizations of the molecule. It is an excellent method in the designing of novel NLO molecules and support to predict some molecular properties such as dipole moment, polarizabilities and hyperpolarizabilities. Among several computational methods, Density Functional Theory (DFT) an efficient tool to provide great accuracy to calculate electronic structure of molecular systems and to reproduce the experimental values in dipole moments, chemical hardness, atomic charges, electron negativity, etc., [21, 22]. In the present investigation, the authors were concentrated and succeeded in the synthesis and single crystal growth of 2-naphthol substituted Mannich base from an active nitrogen compound with suitable secondary amine and an aromatic aldehyde for NLO application such as second harmonic generation. Slow evaporation technique was employed to

achieve optically good quality single crystals of the synthesized compound. The crystalline compound was confirmed by single crystal XRD, FTIR and NMR spectroscopic studies. The grown crystals were also characterized by optical, laser damage and quantum chemical calculations and reported for the first time.

2. Experimental procedure

2.1. Material Synthesis and Growth

All the starting materials and solvent used for the synthesis of MPMN ligand were purchased from Merck chemical company and used without further purification. The ligand MPMN was synthesized successfully using the reactants 2-naphthol, morpholine and benzaldehyde by taking in the equal molar ratio (1:1:1). The active nitrogen compound 2-naphthol (4.33 g, 0.03 M) was dissolved first in a small amount of ethanol and then it was mixed with secondary amine morpholine (2.7 ml, 0.03 M) by a continuous stirrer at room temperature until a clear solution was obtained. Thereafter benzaldehyde (3.0 ml, 0.03 M) was added slowly to this mixture with constant stirring. After 12 hours a brown colored salt was precipitated and it was washed with distilled water for several times and then dried in a hot air oven at 60 °C. The scheme of reaction is as shown in Figure 1. The separated synthesized material was dissolved in the various solvent to obtain the defect-free good quality single crystal. Among the various solvents, acetonitrile was selected as a better solvent to grow the optically good quality single crystal. The separated synthesized material was recrystallized from acetonitrile by the slow evaporation method and a single crystal of dimension 10 x 5 x 2 mm³ was obtained in a period of 20 - 25 days. Figure 2 shows the photograph of an as-grown single crystal of MPMN.

2.2. Characterization

The crystallographic data of MPMN were collected at 293 K by an ENRAF NONIUS CAD4 –MV31 single crystal X-ray diffractometer [λ (Mo $K\alpha$) = 0.71073Å]. The powdered specimen of MPMN single crystal was subjected to FTIR analysis by using PERKIN ELMER/SPECTRUM 2- Fourier Infrared Spectrometer and various functional groups are identified. The ^1H NMR and ^{13}C NMR data of MPMN were recorded in DMSO- d_6 using BRUKER AVANCE III 500 MHz (AV 500) multi nuclei solution NMR Spectrometer. The UV-Visible spectrum of the compound was recorded by using UV/VISIBLE/SPECTROPHOTOMETER - (LAMBDA35 PERKIN ELMER) in the wavelength range between 190 and 1100 nm. The chemical etched pattern of grown crystal of MPMN was examined by EUROMAX optical microscope under transmission mode. The non-linear optical property such as Second Harmonic Generation (SHG) was examined by the Kurtz and Perry powder technique [23]. The intensity of Nd: YAG laser was measured in order to measure the laser damage threshold of MPMN single crystal along (110) plane. The quantum chemical calculations of MPMN were carried out using the Gaussian 09 program package [24] with familiar DFT using Becke's three-parameter hybrid method with the Lee, Yang and Parr correlation functional methods (DFT-B3LYP) at the level of POPLE basis set 6-31G (d, p). For DFT calculations the structure of MPMN molecule was optimized by feeding its experimental Crystallographic Information File (CIF) and all other calculations were computed by the optimized structure of MPMN.

3. Results and discussion

3.1. Single crystal X-ray diffraction study

Single crystal X-ray diffraction is one of the most powerful techniques of unambiguously determines the complete three-dimensional structures of crystals. It is employed for finding unit cell parameters, space groups, and three-dimensional coordinates of atoms and molecules in the unit cell [25]. X-ray crystallography has emerged as the main source of the information on the solids and molecular structure of the compound. The single crystal of MPMN with dimensions $0.35 \times 0.35 \times 0.30 \text{ mm}^3$ was chosen for X-ray diffraction study. The structure of MPMN was solved by the direct method using SHELXS-97 [26] and refined by the full-matrix least squares methods on F^2 using SHELXL-97 [27]. The molecular structure with atom numbering scheme of MPMN at 50 % thermal displacement ellipsoid and optimized geometrical structure is shown in Figure 3. The calculated unit cell parameters are $a = 10.6592 \text{ \AA}$, $b = 18.9868 \text{ \AA}$, $c = 16.7475 \text{ \AA}$, $\alpha = 90^\circ$, $\beta = 101.087^\circ$, $\gamma = 90^\circ$. The unit cell volume is found to be 3326.2 \AA^3 . The obtained lattice parameters are in good agreement with the reported values [28]. From the single crystal XRD studies, it has been found that the compound molecule crystallizes in a monoclinic crystal system with non-centrosymmetric space group Cc. The other crystallographic information and structure refinement for MPMN is provided in Table 1.

There are two independent molecules (**A** & **B**) in the asymmetric unit of the crystallized compound MPMN. The molecular structures of the asymmetric parts of the MPMN are stabilized through two classical intramolecular O—H...N interactions [43O-45H...42N from **A**, 43O-45H...42N from **B**]. Whereas, due to the lack of suitable donor and acceptor atoms for classical intermolecular hydrogen bonds, the crystal packing is stabilized through intermolecular C—H...O interactions. These C—H...O interactions lead to primary chain motifs, which are further

connected and form chain motifs around inversion centers of the unit cell [29]. Hydrogen bonding geometries are given in Table 2. Two interactions of 4C-5H...44O (i) and 7C-8H...44O (i) from **A** leads to two chain C(10) motifs extending along b-axis of the unit cell and a ring $R_2^1(6)$ motif (Figure 4). Further, 4C-5H...44O (i) and 9C-10H...43O (ii) interactions from **B** lead to two chain C(8) and C(10) motifs extending along a- and b-axes of the unit cell, respectively. Further, these two primary chain motifs are intersected leading to secondary ring $R_6^6(46)$ motif (Figure 5). Another chain C(10) motif extending along ab-plane of the crystal is observed through 24C-25H...44O (iii) interaction from **B**. This chain C(10) motif and a chain along the a-axis C(8) motif [4C-5H...44O (i)] from **B** are overlapped and form a ring $R_4^4(32)$ motif (Figure 6). These secondary ring motifs are stabilizing the crystal structure in a greater extent.

The six member ring of morpholine moiety in MPMN adopts a chair conformation with the evident of ring puckering parameters [30] ($Q = 0.576(2) \text{ \AA}$; $\theta = 180.00(19)^\circ$ and $\phi = 2(5)^\circ$) and $q_2 = 0.0240(19) \text{ \AA}$; $q_3 = -0.577(2) \text{ \AA}$). It can also be described by the cyclic torsion angles 30C-33C-44O-36C = $57.8(2)^\circ$, 36C-39C-42N-30C = $-57.8(2)^\circ$, 33C-30C-42N-39C = $58.1(2)^\circ$, 39C-36C-44O-33C = $-57.9(2)^\circ$, 42N-30C-33C-44O = $-59.2(5)^\circ$ and 44O-36C-39C-42N = $59.4(2)^\circ$. Each atom in six member ring of morpholine moiety are deviated from the mean plane of MPMN, viz., 42N = $0.248(16) \text{ \AA}$, 30C = $-0.242(2) \text{ \AA}$, 33C = $0.228(2) \text{ \AA}$, 44O = $-0.221(17) \text{ \AA}$, 36C = $0.229(2) \text{ \AA}$, 39C = $-0.243(2) \text{ \AA}$ which ensures the chair confirmation [31].

The selected bond lengths, bond angles and torsion angles for MPMN are listed in Table 3. As can be seen from the Table the bond lengths and bond angles are extremely closed and slightly longer than the experimental values. The torsion angle for 16C-17C-42N-39C is experimentally observed as $172.83(15)^\circ$ and $67.03(17)^\circ$ from **A** and **B** whereas, the theoretical computation shows this value as 67.036° for lower energy conformation of the molecule. The conformation of

the morpholine moiety shows large value for its conformation angle for lower energy confinement. The dihedral angles between phenyl and naphthyl ring moieties obtained as 15C-16C-17C-19C = 85.42 (19) °, 1C-16C-17C-19C = -88.43 (19) ° from **B** and 15C-16C-17C-19C = -87.40 (19) °, 1C-16C-17C-19C = 89.5 (2) ° from **A** which are nearly equal to the reported values [28] such as 11C-17C-10C-9C = 85.6 (2) °, 11C-17C-10C-1C = -88.9 (2) ° and 19C-18C-34C-28C = -87.8 (2) °, 23C-18C-34C-28C = 89.8 (3) °. The differences between the experimental and calculated geometrical parameters can be attributed due to the fact that the theoretical calculations were carried out with isolated molecules in the gaseous phase while the experimental values were based on the molecules in the solid state are different in nature. The crystallographic data (CIF) for the molecule compound structure reported in this paper have been deposited in the Cambridge Crystallographic Data Centre as supplementary material number CCDC 1029398.

3.2. FT-IR analysis

FT-IR spectrum of MPMN recorded in KBr medium in the spectral range (4000-400 cm^{-1}) which exhibited a number of bands as shown in Figure 7. The compound shows a number of IR absorption bands and the absorption frequencies are in a slightly shifted position in comparison with those of the reactants, 2-naphthol, and morpholine. A broadband observed at 3404 cm^{-1} is assigned to the $\nu_{\text{O-H}}$ stretching vibration. The aromatic stretching ν_{CH} occurs at 3058 cm^{-1} .

The absorption band due to asymmetric and symmetric stretching vibration of alicyclic ν_{CH_2} occurs at 2966 and 2842 cm^{-1} . The $\nu_{\text{C=C}}$ stretching vibration occurs at 1598 and 1470 cm^{-1} . The δ_{OH} in-plane bending and $\nu_{\text{ring}} + \delta_{\text{CH}}$ vibrations appear at 1236, 1414 and 1454 cm^{-1} respectively. A small and sharp absorption band observed around 747 cm^{-1} may be due to phenyl ring out of plane bending vibration. The $\nu_{\text{C-N-C}}$ and $\nu_{\text{C-O-C}}$ stretching vibrations occur at 1157,

1143 and 1093 cm^{-1} . The absorption band due to the newly formed C-N-C appears at 1115 cm^{-1} which favorably indicates the substitution on 2-naphthol and morpholine and the formation of a new compound. The FT-IR data was also obtained theoretically by GAUSSIAN using frequency command and it is shown all vibrational modes observed as real with positive frequencies. The data is given as supplementary information.

3.3 ^1H NMR, ^{13}C NMR – analysis

The ^1H NMR data for the compound MPMN in DMSO-d_6 is shown in Figure 8. The multiplet observed at δ 7.204 – 7.303 ppm is attributed to the protons of the phenyl ring. The O- CH_2 and N- CH_2 proton of morpholine observed as two triplets at δ 3.564 and 2.499 ppm respectively. The CH protons of the naphthyl ring appear as a doublet and multiplet at 7.102 and 7.619-7.749 ppm respectively. The OH proton appears as a singlet 13.181 ppm, whereas the methane CH proton appears at 5.360 ppm. The signal of the methine CH proton indicates the formation of a new compound.

The ^{13}C NMR spectrum of the compound MPMN was recorded in DMSO-d_6 and is shown in Figure 9. The ^{13}C NMR data for the title compound in DMSO-d_6 shows the chemical shifts of phenyl ring carbons 1', 2' & 6', 3' & 5' and 4' appears at δ 139.837, 128.727, 229.789 and 129.212 ppm respectively. The signals observed at δ 52.423 and δ 66.566 ppm is due to the N- CH_2 and O- CH_2 carbons of morpholine. The signal for the naphthyl carbons 1'- 10' appears at δ 109.120, 154.903, 116.167, 128.341, 127.992, 122.003, 126.583, 123.001, 132.503 and 129.094 ppm respectively. The signal for the newly formed CH carbon occurs at δ 70.390 ppm, which imitates the formation of a new compound. The ^{13}C NMR signals of the compound and the various assignments to the different carbon atoms are in good agreement with the ^1H NMR data.

3.4. UV-Vis-NIR studies

A good optical transmittance is a very desirable property for an NLO crystal [32]. A well polished and transparent single crystal of MPMN with 2 mm thickness was used for the UV-vis absorption studies. The plot of absorbance versus wavelength with inset of Tauc's plot is shown in Figure 10. There is no absorption peak observed between 360 and 1100 nm, the lower cutoff wavelength is observed at 228.09 nm and 354.02 nm for MPMN and the lower percentage of absorption indicates that the crystal readily allows the transmission of the laser beam in the range between 360 nm and 1100 nm. The optical absorption bands at 228.09 nm and 354.02 nm can be assigned to π to π^* and n to π^* electronic transitions of aromatic groups of MPMN. From the observations, it is understood that the grown crystal has a good transparency in UV, visible, and near-IR region indicating that it can be used for various NLO applications [33]. The Tauc's plot [34] was drawn between the photon energy ($h\nu$) and $(\alpha h\nu)^2$ and used to estimate the energy band gap of the crystalline material. It was determined by extrapolating the straight line portion of the curve to $(\alpha h\nu)^2 = 0$. From the plot, the optical energy band gap of MPMN is estimated as 3.3 eV.

3.5. Etching

The nonlinear optical efficiency of a crystal mainly depends on the quality of the grown crystal. The presence of impurities and dislocations during growth may affect the quality of the grown crystal. The chemical etching is a significant method for revealing the crystal defects that are affected by such as chemical homogeneity, electron mobility, light absorption, refractive index and stress [35]. It can able to develop some feature such flat-bottomed pits, etch hillocks, and etch spirals on the surface of the crystal. The etch pits are developed due to chemical attack of the etchants at the strain field surrounding the dislocation line. The shape, size, and orientation of the pits can be related to the crystal symmetry [36]. In the present study grown MPMN single

crystal was fully immersed in ethanol etchant for 20 and 40 seconds at room temperature. The etched surfaces were dried gently by pressing them between filter papers and immediately examined the microstructure surface using computerized optical microscope by transmission mode. The microphotographs of the crystal plane (110) before and after etching is shown in Figure 11. From the Figure, the rectangular etch pits were observed at the site of dislocations in 20 seconds. The etching time increases by 40 seconds, the size of the etch pits were also increased which confirms that the size of the etch pattern increases with increase in etching time. The etch pits density was calculated as 786 cm^{-2} from etch pattern formed at 40 seconds after etching. There is no change was found in the size of etch pits over 40 seconds, which suggest that the etch pits are due to dislocations.

3.6. NLO test

Kurtz and Perry powder technique represents the first real means of screening, experimentally large number of unknown materials for second order nonlinear optical activity [23]. In this technique, the grown crystalline compound was ground into a fine microcrystalline powder and was filled into a fine microcapillary tube of diameter 1.4 mm. The filled microcapillary tube was taken along the path of Nd: YAG laser operated at 1.9 mJ/pulse energy with the fundamental wavelength 1064 nm with 8 ns pulse width at a repetition rate of 10 Hz. The second harmonic radiation generated by the randomly oriented microcrystals was focused by a lens and detected by a photomultiplier tube and digitalizing oscilloscope assembly. The final output was displayed on a digital storage oscilloscope and the second harmonic signal generated was confirmed from the emission of bright green light of wavelength 532 nm from the powdered sample cell. The output second harmonic signal of 58 mV, 37 mV were obtained from MPMN,

standard inorganic KDP crystal powder. The conversion efficiency of MPMN sample is found to be 1.57 times greater than KDP from the observed result.

3.7. Laser damage threshold

For NLO device applications, laser damage threshold plays a significant role. The usage of NLO crystal depends not only on the linear and nonlinear optical properties but also its ability to withstand for high power lasers [37]. Usually, organic crystal shows a very high damage threshold value compared to inorganic counterpart [38]. The laser damage threshold studies have been carried out for MPMN single crystal using a Q-switched Nd: YAG laser ($\lambda = 1064 \mu\text{m}$) of multishot with the pulse duration of 10 ns at a frequency rate of 10 HZ. The lens with focal length of 35 cm was used to position the different sites in the laser beam. The laser beam of 1 mm was focused on the polished face of the MPMN along (110) plane. The applied input energy of laser was increased gradually and at 79 mJ the cracks were developed on the surface of MPMN single crystal. The power density (P_d) was calculated using the formula,

$$P_d = \frac{E}{\tau A} \quad \text{--- (1)}$$

Where E is the input energy measured in millijoules, τ is the pulse width and A is the area of the circular spot. The measured multiple shots surface damage threshold value is 1.006 GW/cm^2 . The laser induced damage pattern of MPMN shows (Figure 12) cracks developed around the core of damage with small blobs. These damages are mainly due to the thermal effects such as heat induced by the absorption of the laser radiation, multiphoton ionization and thermal diffusivity of MPMN which was resulting in melting, solidification, and decomposition of the material [39].

3.8. Quantum chemical calculation

3.8.1 Non-Linear Optical Properties

The Quantum chemistry based calculation of non-linear optical properties of a molecule has a significant role for the design of materials in modern communication technology and optical signal processing [40]. It gives an important contribution to the understanding of the electronic polarization underlying the molecular NLO process and the structure-property relationship [41]. The quantum chemical calculations of polarizabilities and hyperpolarizabilities have become available through the strong theoretical basis for analyzing molecular interactions. They made the possible determination of the elements of these tensors from derivatives of the dipole moment with respect to finite field approach. DFT is an efficient method for providing a suitable theoretical framework and structure sensitive method for calculating molecular polarizabilities, dipole moment and electronic charge distribution extracted from the output of any standard electronic structure program.

The total static dipole moment (μ), the mean polarizability (α), the anisotropy polarizability ($\Delta\alpha$) and first hyper polarization (β) using the components x, y, z are given below,

$$\text{Total static dipole moment } \mu = \sqrt{\mu_x^2 + \mu_y^2 + \mu_z^2} \quad \text{--- (2)}$$

$$\text{The mean polarizability } \alpha = \frac{\alpha_{xx} + \alpha_{yy} + \alpha_{zz}}{3} \quad \text{--- (3)}$$

$$\text{The anisotropy of polarizability } \Delta\alpha = \frac{1}{\sqrt{2}} \sqrt{(\alpha_{xx} - \alpha_{yy})^2 + (\alpha_{yy} - \alpha_{zz})^2 + (\alpha_{zz} - \alpha_{xx})^2 + 6\alpha_{xx}^2} \quad \text{--- (4)}$$

The first order hyperpolarizability is a third-rank tensor that can be described by a 3x3x3 matrix. Accordance with Kleinman symmetry the 27 components of the 3D matrix can be reduced to 10 components [42]. The complete equation for calculating the magnitude of the first order hyperpolarizability as follows,

$$\beta = \sqrt{(\beta_{xxx} + \beta_{xyy} + \beta_{xzz})^2 + (\beta_{yyy} + \beta_{xxy} + \beta_{yzz})^2 + (\beta_{zzz} + \beta_{xxz} + \beta_{yyz})^2} \quad \text{--- (5)}$$

Since the values of the polarizability and hyperpolarizability of the GAUSSIAN 09 output are reported in atomic units (a.u), the calculated values have been converted into electrostatic units (esu) (α : 1 a.u. = 0.1482×10^{-24} esu; β : 1 a.u. = 8.641×10^{-33} cm⁵ esu⁻¹). The calculated values of μ , α , $\Delta\alpha$ and β for MPMN calculated were 1.6863 D, 23.9211×10^{-24} esu, 73.0372×10^{-24} esu and 2.1191×10^{-30} cm⁵ esu⁻¹ and compared with the prototypical molecule like urea. Since urea is one of the prototypical molecules used in the study of NLO properties of molecular systems, it was used frequently as the threshold value for comparative purpose. The polarizability, anisotropy polarizability and first order hyperpolarizability of MPMN were observed 8.3966, 5.8759 and 5.2452 times greater than the urea molecule in the gas phase.

3.8.2 Frontier molecular orbital (FMO) analysis

The HOMO and LUMO are often called as frontier molecular orbital. The frontier molecular orbital is mainly composed of π -atomic orbital so that an electron transition from the HOMO to the LUMO is mainly derived from $\pi - \pi^*$ electronic transition. The FMO analysis indicates that the transition of the electron from ground to first excited state and is mainly described by one electron excitation for the highest occupied molecular orbital (HOMO) to the lowest unoccupied orbital (LUMO). The molecular energies of HOMO and LUMO have been calculated as 5.3783 and -0.9082 eV and the plots are given in Figure 13 respectively. The energy gap between HOMO and LUMO was found to be 4.4701 eV which indicates that the title compound having higher energy barrier for the transition of electrons from highly occupied molecular orbital to lowest unoccupied molecular orbital. The partaking of each fragment of MPMN and their HOMO and LUMO percentage is calculated using the QMForge software tool [43]. In MPMN, 92 % of HOMO and 85 % of LUMO are significantly contributed by the

naphthyl moiety (F-I), which implies the maximum electronic charge transfer takes place through the fragment molecule which is essential requirement to obtain the large second order NLO response. The difference between the theoretical and experimental values (UV-Vis-optical absorbance) of energy barrier is due to the isolated molecule of MPMN in a gas phase and the three-dimensional crystalline solid is different in nature.

Accordance with Koopman theorem [44], the chemical hardness (η), the electronic chemical potential (μ) and electrophilicity index (ω) of MPMN can be calculated as below. The chemical hardness is associated with the stability and reactivity of a chemical system. The smaller in energy gap implies soft molecules where large energy gap leads harder molecule. In a molecule, it measures the resistance to change in the electron distribution or charge transfer. Based on frontier molecular orbital, chemical hardness (η) corresponds to the gap between the HOMO and LUMO.

$$\eta = \frac{(E_{\text{LUMO}} - E_{\text{HOMO}})}{2} \quad \text{--- (6)}$$

Where E_{LUMO} and E_{HOMO} are the energies of LUMO and HOMO. The larger the HOMO-LUMO energy gap, the harder and more stable/less reactive molecule.

The electronic chemical potential is defined as the negative of electronegativity of a molecule which describes the escaping tendency of the electron from an equilibrium system. It is determined as,

$$\mu = \frac{(E_{\text{HOMO}} + E_{\text{LUMO}})}{2} \quad \text{--- (7)}$$

Electrophilicity index measures the capacity of a species to accept electrons [45]. It is the measure of the stabilization in energy after a system accepts additional amount of electronic charge from the environment which is given as,

$$\omega = \frac{\mu^2}{2\eta} \quad \text{--- (8)}$$

The chemical hardness, electrochemical potential, and electrophilicity index of MPMN were obtained from FMO analysis are 2.2350, -3.1432 and 2.2102 eV. From the results, it could be observed that the title compound molecules possess good chemical hardness in nature [46].

3.8.3 Molecular electrostatic potential

The total electrostatic effect or field produced at a point in space around a molecule due to net charge distribution electron and nuclei is termed as molecular electrostatic potential $V(r)$ (MEP). It is expressed as below [47],

$$V(r) = \sum_A \frac{Z_A}{|R_A - r|} - \int \frac{\rho(r') dr'}{|r' - r|} \quad \text{--- (9)}$$

Where Z_A is the charge on nucleus located at distance R_A and $\rho(r)$ is the electron density. The MEP is correlated with dipole moments, electronegativity and chemical reactivity of the molecule. It gives the visual inspection of the polarity of the molecule. The electrostatic potential region was taken between $-1.366 \times e^{-2}$ and $1.366 \times e^{-2}$ and the map is shown in Figure 14. The electrostatic potential surface of the molecule can be represented by different color grading. The red represents the most negative electrostatic potential region, whereas blue represents the most positive electrostatic potential region and green represent the region of zero potential. The negative electrostatic potential corresponds to an attraction of proton by the concentrated electron in the molecules which give the electrophilic attack or reactive sites of the molecular system. The positive electrostatic potential corresponding to the repulsion of the proton by atomic nuclei in the regions of low electron density excites which gives nucleophilic attack or reactive sites of the molecular system. These sites give the information about the region from where the compound can have intermolecular interaction.

3.8.4 Mulliken charge analysis

The total atomic charges of MPMN molecule obtained from Mulliken charge population by DFT method. Atomic charges play a vital role in quantum chemistry and more research continues to be done to refine the concept of an atomic charge. Mulliken atomic charge populations give one of the simplest pictures of charge distribution and predict the net atomic charges in the molecule [48]. The charge distribution of all atoms in the investigated molecule is shown in Figure 15. Also from the Figure, it could be observed that the atomic charges of the molecule are ranging between 0.3441 and -0.6015. The highest value is observed at C1 and H45 atom, where the lowest value is observed in N42, O43, and O44 atoms. Almost maximum hydrogen atoms exhibited positive charge, whereas the maximum of carbon and nitrogen atoms possess the negative charge.

4. Conclusion

2-naphthol substituted Mannich base MPMN was synthesized and crystallized successfully using suitable acetonitrile solvent by slow evaporation method at room temperature. The single crystal XRD confirms that the MPMN crystallizes in monoclinic crystal system with the non-centrosymmetric space group Cc. The different vibrational modes of functional groups are presented in MPMN were confirmed by FTIR analysis. The ^1H NMR and ^{13}C NMR confirms the formation of a new compound by the observed signal of the methine CH proton at 5.360 ppm and the signal occurs at δ 70.390 ppm due to CH carbon. The UV-Vis absorption spectrum confirms, the lower cutoff wavelengths observed at 228.09 nm and 354.02 nm which ensures wider optical transparency range in entire visible and near infrared region. The chemical etching pattern formed by the suitable etchant revealed that MPMN single crystal has minimum dislocation sites during growth. The SHG response of MPMN crystal revealed that the efficiency

is 1.57 times greater than KDP which ensures the crystal can be suitable for NLO applications. The laser damage threshold of MPMN was found to be 1.006 GW/cm^2 . The quantum chemical studies revealed the favorable NLO response in the dipole moment, molecular polarizability, hyperpolarizability and chemical hardness of MPMN in the gas phase.

Reference

- [1] N. Zaitseva, and L. Carman, Rapid growth of KDP-type crystals, *Prog. Crystal Growth and Charact.* 43 (2001) 1-118.
- [2] X.J. Liu, Z.Y. Wang, X.Q. Wang, G.H. Zhang, S.X. Xu, A.D. Duan, S.J. Zhang, Z.H. Sun, D. Xu, Morphology and Physical Properties of L-Arginine Trifluoroacetate Crystals, *Cryst. Growth Des.* 8 (2008) 2270–2274.
- [3] J. Badan, R. Hierle, A. Perigaud, J. Zyss, NLO properties of Organic Molecules and Polymeric Materials, ACS Symp. Ser. 233, Am. Chem. Soc. Washington, DC, 1993.
- [4] P.N. Prasad, Polymeric Materials for Nonlinear Optics and Photonics, *Polym.* 32 (1991) 1746-1751.
- [5] B.G. Penn, B.H. Cardelino, C.E. Moore, A.W. Shields, D.O. Frazier, Growth of bulk single crystals of organic materials for nonlinear optical devices: An overview, *Prog. Cryst. Growth Charact.* 22 (1991) 19-51.
- [6] B.E.A. Saleh, M.C. Teich, *Fundamental of Photonics*, Wiley, New York, 1991.
- [7] S.R. Marder, S.E. Sohn, G.D. Stucky, *Material for Nonlinear Optics Chemical Perspective*, ACS Symp. Ser. 455, Am. Chem.Soc. Washington, DC, 1991.
- [8] Venkataraya Shettigar, P.S. Patil, S. Naveen, S.M. Dharmaprakash, M.A. Sridhar, J. Shashidhara Prasad, Crystal growth and characterization of new nonlinear optical chalcone derivative: 1-(4-Methoxyphenyl)-3-(3, 4-dimethoxyphenyl)-2-propen-1-one, *J. Cryst. Growth* 295 (2006) 44-49.
- [9] D.R. Kanis, M. A. Ratner, T.J. Marks, Design and construction of molecular assemblies with large second-order optical nonlinearities. Quantum chemical aspects, *Chem. Rev.* 94 (1994) 195-242.

- [10] T. Pal, T. Kar, Gabriele Bocelli, Lara Rigi, Synthesis, Growth, and Characterization of L-Arginine Acetate Crystal: A Potential NLO Material, *Cryst. Growth Des.* 3 (2003) 13-16.
- [11] V. Krishnakumar, R. Nagalakshmi, Vibrational spectroscopic studies of an organic non-linear optical crystal 8-hydroxyquinolinium picrate, *Spectrochim. Acta Part A*, 66 (2007) 924-934.
- [12] N. Vijayan, R. Ramesh Babu, M. Guneseakaran, R. Gopalakrishnan, R. Kumarasan, P. Ramasamy, C.W. Lan, Studies on the growth and characterization of *p*-hydroxyacetophenone single crystals, *J. Cryst. Growth*, 249 (2003) 309-315
- [13] M. Kosal, N. Gokhan, E. Kupeli, E. Yesilada, H. Erdogan, Analgesic and anti-inflammatory activities of some new Mannich bases of 5-nitro-2-benzoxazolinones, *Arch. Pharm. Res.* 30 (2007) 419-424.
- [14] J.R. Dimmock, N.M. Kandepu, U. Das, G.A. Zello, K.H. Nienaber, Antimycobacterial arylidenecyclohexanones and related Mannich bases, *Pharmazie*, 59 (2004) 502-505.
- [15] S.C. Vashishtha, G.A. Zello, K.H. Nienaber, J. Balzarini, E. De Clercq, J.P. Stables, J.R. Dimmock, Cytotoxic and anticonvulsant aryloxyaryl Mannich bases and related compounds, *Eur. J. Med. Chem.*, 39 (2004) 27-35.
- [16] E. Bennet-Jenkins, C. Bryant, Novel sources of anthelmintics, *Int. J. Parasitol.*, 26 (1996) 937-947.
- [17] M. Tramontini, L. Angiolini, *Mannich Bases - Chemistry and Uses*, CRC Press, 1994.
- [18] M. Jeeva, G. Venkatesa Prabhu, M.S. Boobalan, C.M. Rajesh, Interactions and Inhibition Effect of Urea-Derived Mannich Bases on a Mild Steel Surface in HCl, *J. Phys. Chem. C* 119 (2015) 22025-22043.
- [19] M. Betti, Synthesis of Betti base, *Org. Synth. Collective 1* (1941) 381-383.

- [20] M. Betti, On the addition of benzyl amine to naphthol, *Gazz. Chim. Ital.* 30 (1900) 301-309.
- [21] M. Amalanathan, I. Hubert Joe, V.K. Rastogi, Density functional theory studies on molecular structure and vibrational spectra of NLO crystal L-phenylalanine phenylalanium nitrate for THz application, *J. Mol. Struct.* 1006 (2012) 513-526.
- [22] Y. Koysal, H. Tanak, Crystal structure, spectroscopic investigations and density functional studies of 4-(4-methoxyphenethyl)-5-benzyl-2H-1,2,4-triazol-3(4H)-one monohydrate, *Spectrochim. Acta Part A* 93 (2012) 106– 115.
- [23] S.K. Kurtz, T.T. Perry, A Powder Technique for the Evaluation of Nonlinear Optical Materials, *J. Appl. Physics*, 39 (1968) 3798-3813.
- [24] M.J. Frisch, G.W. Trucks, H.B. Schlegel, G.E. Scuseria, M.A. Robb, J.R. Cheeseman, G. Scalmani, V. Barone, B. Mennucci, G.A. Petersson, H. Nakatsuji, M. Caricato, X. Li, H.P. Hratchian, A.F. Izmaylov, J. Bloino, G. Zheng, J.L. Sonnenberg, M. Hada, M. Ehara, K. Toyota, R. Fukuda, J. Hasegawa, M. Ishida, T. Nakajima, Y. Honda, O. Kitao, H. Nakai, T. Vreven, J.A. Montgomery, Jr., J.E. Peralta, F. Ogliaro, M. Bearpark, J.J. Heyd, E. Brothers, K.N. Kudin, V.N. Staroverov, T. Keith, R. Kobayashi, J. Normand, K. Raghavachari, A. Rendell, J.C. Burant, S.S. Iyengar, J. Tomasi, M. Cossi, N. Rega, J.M. Millam, M. Klene, J.E. Knox, J.B. Cross, V. Bakken, C. Adamo, J. Jaramillo, R. Gomperts, R.E. Stratmann, O. Yazyev, A.J. Austin, R. Cammi, C. Pomelli, J.W. Ochterski, R.L. Martin, K. Morokuma, V.G. Zakrzewski, G.A. Voth, P. Salvador, J.J. Dannenberg, S. Dapprich, A.D. Daniels, O. Farkas, J.B. Foresman, J.V. Ortiz, J. Cioslowski, and D.J. Fox, Gaussian, Inc., Wallingford CT, 2010.
- [25] G.H. Stout, L. H. Jenson, X-ray Structure determination, Macmillan, Newyork, 1968.

- [26] G.M. Sheldrick, SHELXS-97; Program for crystal structure solution, University of Gottigen, Germany, 1997.
- [27] G.M. Sheldrick, SHELXL-97; Program for refinement of crystal structures, University of Gottigen, Germany, 1997.
- [28] Min Min Zhao and Ping Ping Shi, 1-[Morpholino(phenyl)methyl]-2- Naphthol, Acta Cryst. E66, o1406, (2010).
- [29] J. Bernstein, R.E. Davis, L. Shimoni, and N.L. Chang, Patterns in hydrogen bonding: functionality and graph set analysis in crystals, *Angew. Chem. Int. Ed. Engl.* 34 (1995) 1555–1573.
- [30] D. Cremer, J.A. Pople, General definition of ring puckering coordinates, *J. Amer. Chem. Soc.* 97 (1975) 1354-1358.
- [31] J.C.A. Boeyens, The conformation of six-membered ring, *J. Cryst. Mol. Struct.* 8 (1978) 317-320.
- [32] V.G. Dmitriev, G.G. Gurzadyan, D.N. Nikoyosyan, *Hand Book of Nonlinear Optical Crystals*, Third Revised Edition, Springer Series in Optical Sciences, 64 (1999) 1-413.
- [33] Z.Y. Wang, *Near-Infrared Organic Materials and Emerging Applications*, CRC press, Taylor and Francis group, 2013.
- [34] J. Tauc, R. Grigorovici, A. Vance, Optical properties and electronic structure of amorphous germanium, *Phys. Status Solidi B*, 15 (1966) 627-637.
- [35] X. He, D. Xue, Doping mechanism of optical-damage-resistant ions in lithium niobate crystals, *Opt. Commun.* 265 (2006) 537-541.

- [36] S. Mukerji, T. Kar, Surface Micromorphology of Different Crystallographic Faces of L-arginine Hydrochloride Monohydrate Etched in Organic Solvents, *Jpn. J. Appl. Phys.* 38 (1999) 832-837.
- [37] P. Vijayakumar, G. Anandha Babu, P. Ramasamy, Synthesis, crystal growth and characterization of nonlinear optical organic crystal: p-Toluidinium p-toluenesulphonate, *Mater. Res. Bull.* 47 (2012) 957-962.
- [38] P.S. Patil, M.S. Bannur, D.B. Badigannavar, S.M. Dharmaprakash, Study on nonlinear optical properties of 2,4,5-trimethoxy-4'-bromochalcone single crystal, *Opt. Laser Technol.* 55 (2014) 37-41.
- [39] G. Anandha Babu, P. Ramasamy, Growth and characterization of 2-amino-4-picolinium toluene sulfonate single crystal, *Spectrochim. Acta Part A* 82 (2011) 521-526.
- [40] D. Sajan, H. Joe, V.S. Jayakumar, J. Zaleski, Structural and electronic contributions to hyperpolarizability in methyl p-hydroxy benzoate, *J. Mol. Struct.* 785 (2006) 43-53.
- [41] J.Y. Lee, K.S. Kim, Relationship between spectral intensities and nonlinear optical properties, *J. Chem. Phys.* 107 (1997) 6515-6520.
- [42] D.A. Kleinman, Nonlinear Dielectric Polarization in Optical Media, *Phys. Rev.* 126 (1962) 1977-1979.
- [43] A.L. Tenderholt, QMForge, Version 2.1; Stanford University: Stanford, CA, USA.
- [44] T. Koopmans, Über die Zuordnung von Wellenfunktionen und Eigenwerten zu deneinzeln Elektronen eines Atoms, *Physica* 1 (1934) 104-113.
- [45] R.G. Parr, L. Szentpaly, S. Liu, Electrophilicity Index, *J. Am. Chem. Soc.* 121 (1999) 1922-1924.

- [46] C.A. Mebi, DFT study on structure, electronic properties, and reactivity of cis-isomers of $[(\text{NC}_5\text{H}_4\text{-S})_2\text{Fe}(\text{CO})_2]$, *J. Chem. Sci.* 123 (2011) 727-731.
- [47] P. Politzer and J.S. Murray, The fundamental nature and role of the electrostatic potential in atoms and molecules, *Theor. Chem. Acc.* 108 (2002) 134-142.
- [48] R.S. Mulliken, Electronic population analysis on LCAO-MO molecular wave functions, *J. Chem. Phys.* 23 (1955) 1833-1840.

List of Figures

1. Reaction scheme for the synthesis of Mannich base MPMN
2. Photograph of as grown single crystal of MPMN
3. ORTEP diagram and optimised geometry of MPMN
4. Two chain C(10) motifs extending along b-axis of the unit cell and a ring $R_2^1(6)$ motif of MPMN
5. Chain C(8) and C(10) motifs extending along a- and b-axes leads to secondary ring $R_6^6(46)$ motif of MPMN
6. Primary chain C(8) and C(10) motifs overlapped leading to secondary ring $R_4^4(32)$ motif of MPMN
7. FT-IR spectrum of MPMN
8. ^1H NMR spectrum of MPMN
9. ^{13}C NMR spectrum of MPMN
10. UV-Vis absorption spectrum along with Tauc's plot of MPMN single crystal
11. Etch patterns of MPMN before and after etching
12. Laser damage pattern of MPMN single crystal
13. HOMO and LUMO plot of MPMN
14. Electro Static Potential Map of MPMN
15. Mulliken's charge distribution of MPMN

List of Tables

1. Crystallographic parameters for MPMN single crystal
2. Hydrogen bonding geometry of MPMN from single crystal XRD

3. Comparison between selected optimized geometrical parameters and experimental crystallographic parameters for MPMN
4. Molecular polarizabilities and dipole moment of MPMN

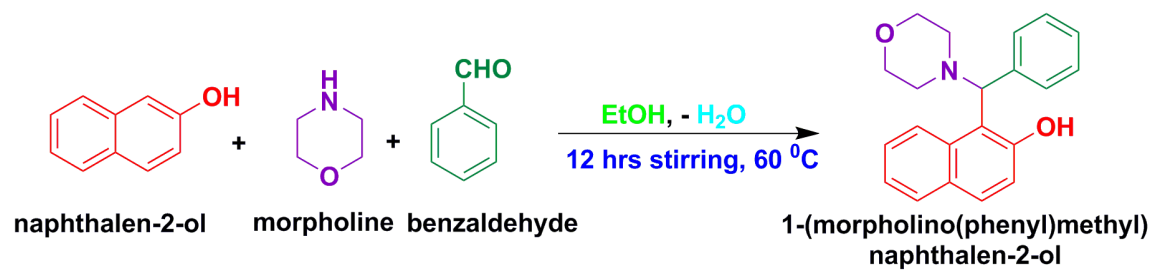


Fig. 1. Reaction scheme for the synthesis of Mannich base MPMN

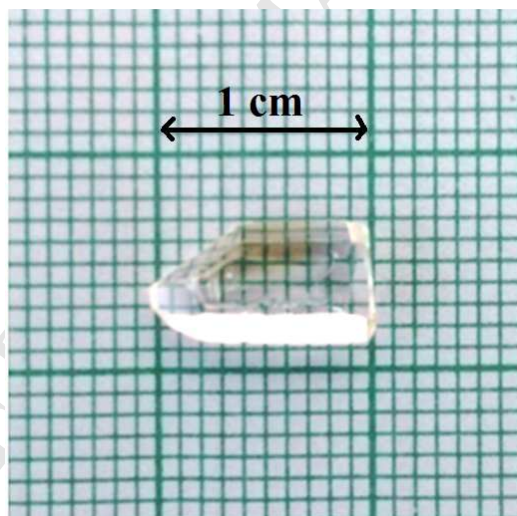


Fig. 2. Photograph of as grown single crystal of MPMN

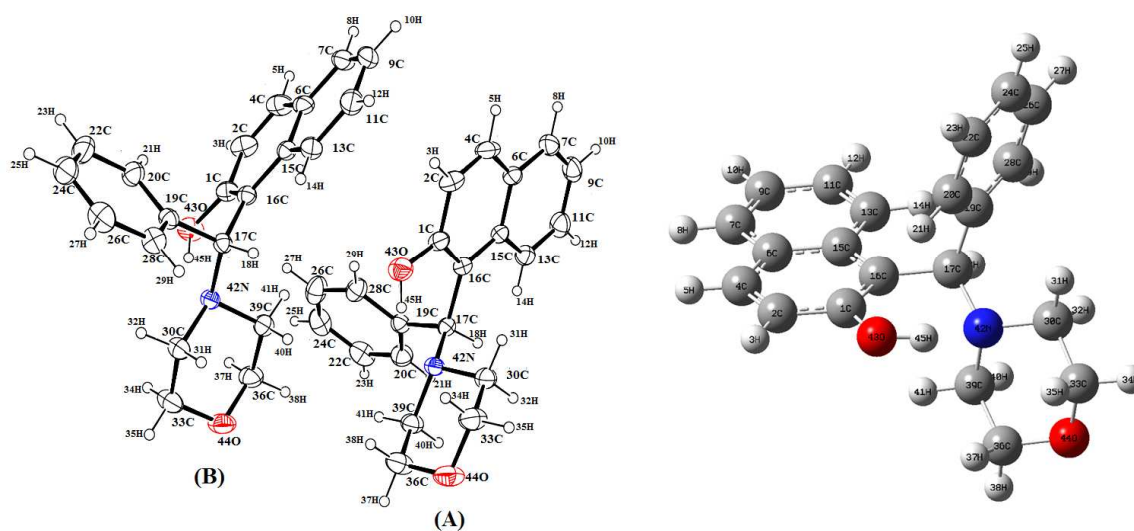


Fig. 3. ORTEP diagram and optimised geometry of MPMN

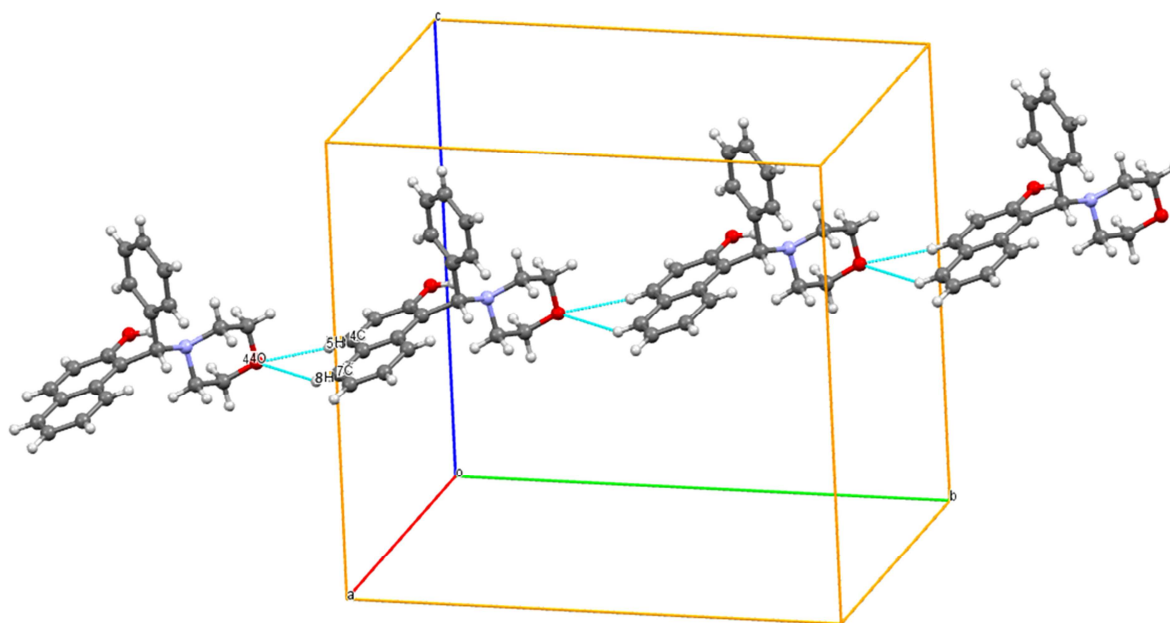


Fig. 4. Two chain C(10) motifs extending along b-axis of the unit cell and a ring R₂¹(6) motif of MPMN

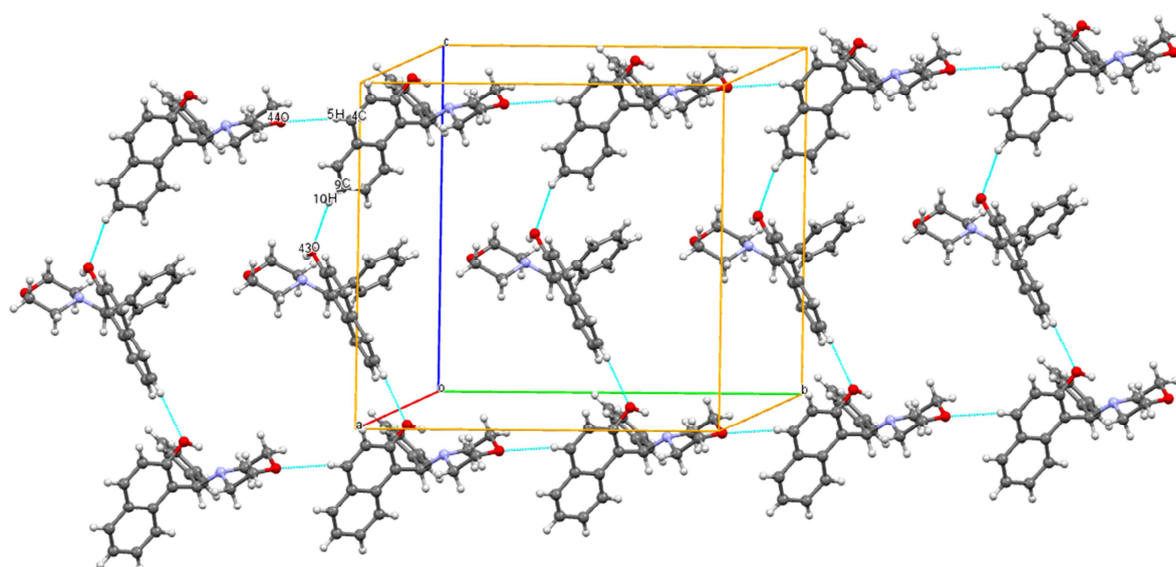


Fig. 5. Chain C(8) and C(10) motifs extending along a- and b-axes leads to secondary ring $R_6^6(46)$ motif of MPMN

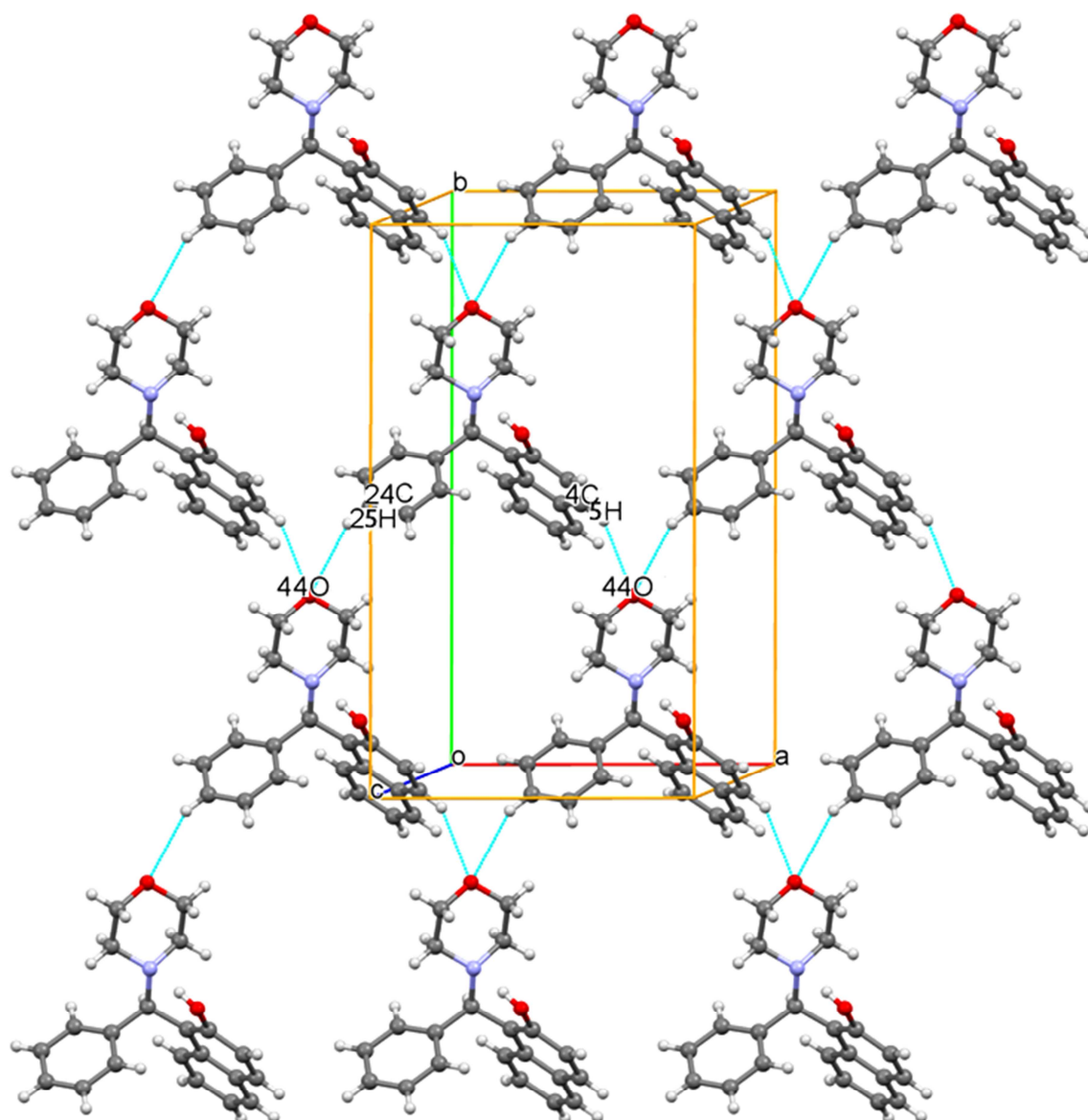


Fig.6. Primary chain C(8) and C(10) motifs overlapped leading to secondary ring $R_4^4(32)$ motif of MPMN

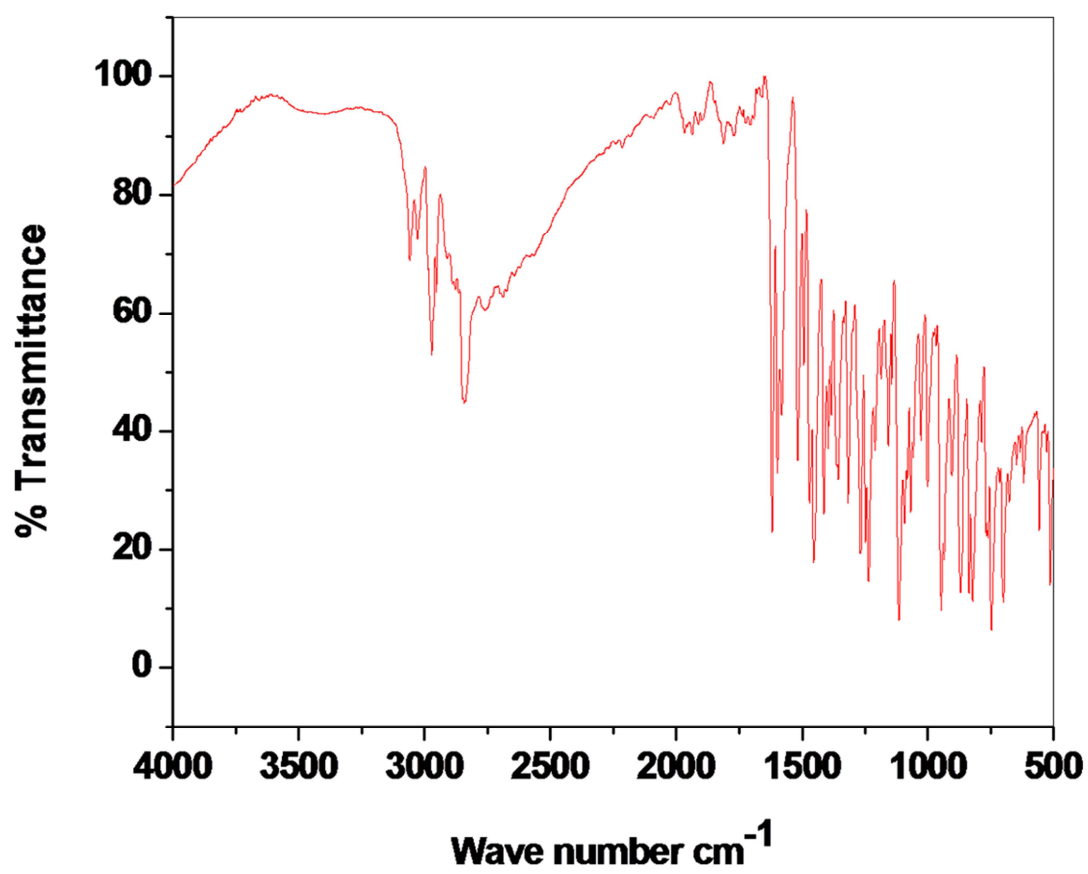


Fig. 7. FT-IR spectrum of MPMN

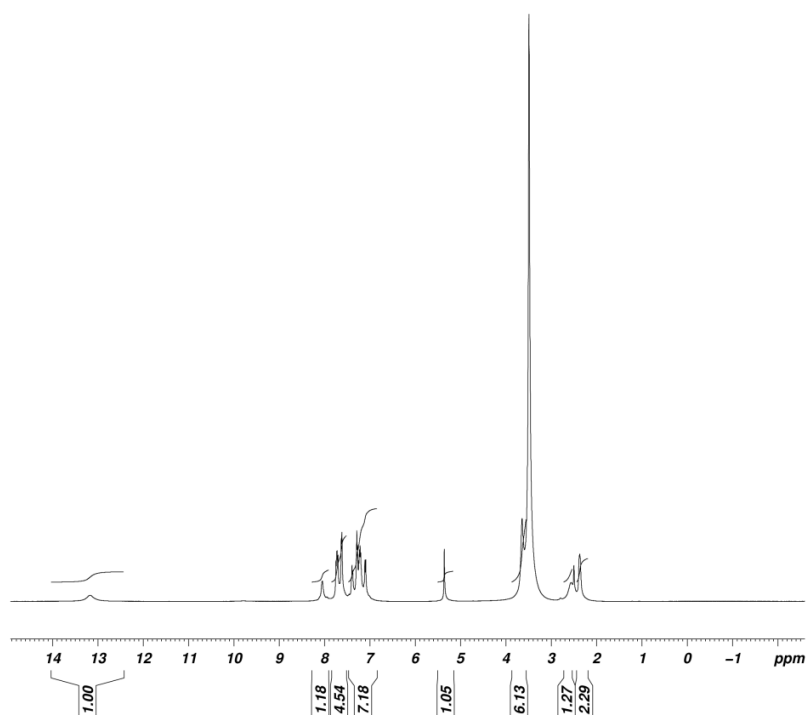


Fig. 8. ^1H NMR spectrum of MPMN

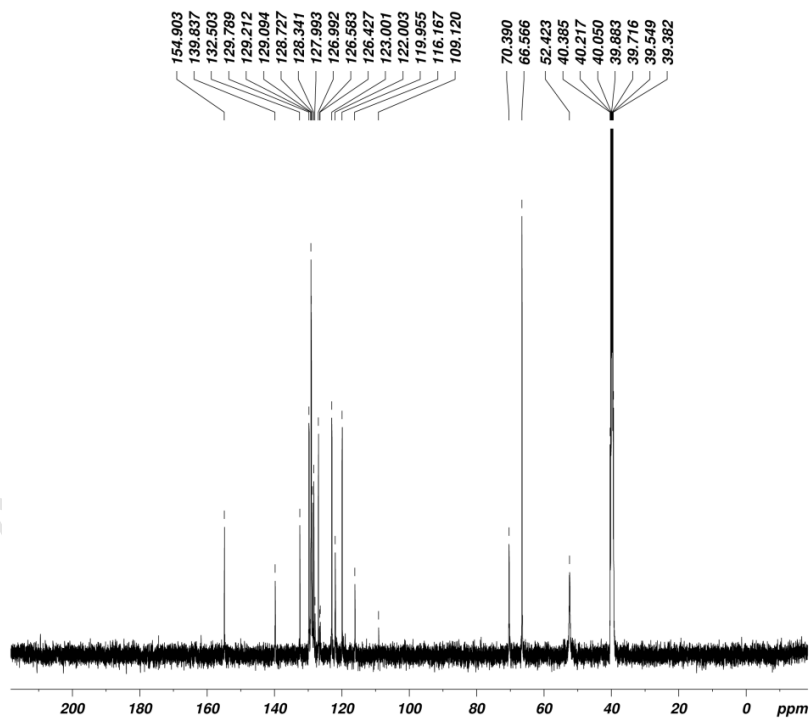


Fig. 9. ^{13}C NMR spectrum of MPMN

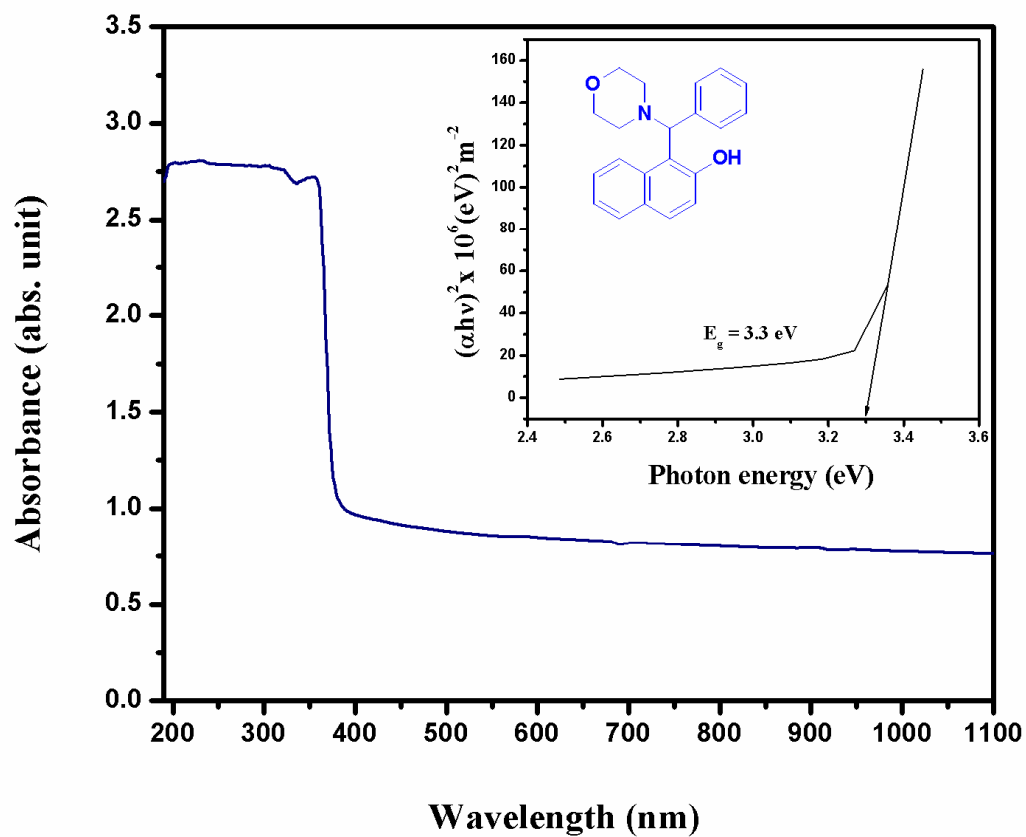


Fig. 10. UV-Vis absorption spectrum along with Tauc's plot of MPMN single crystal

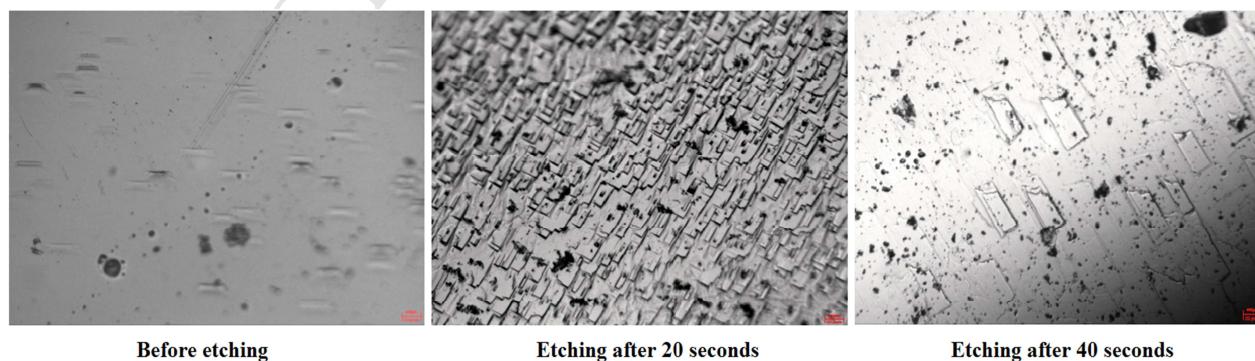


Fig. 11. Etch patterns of MPMN before and after etching

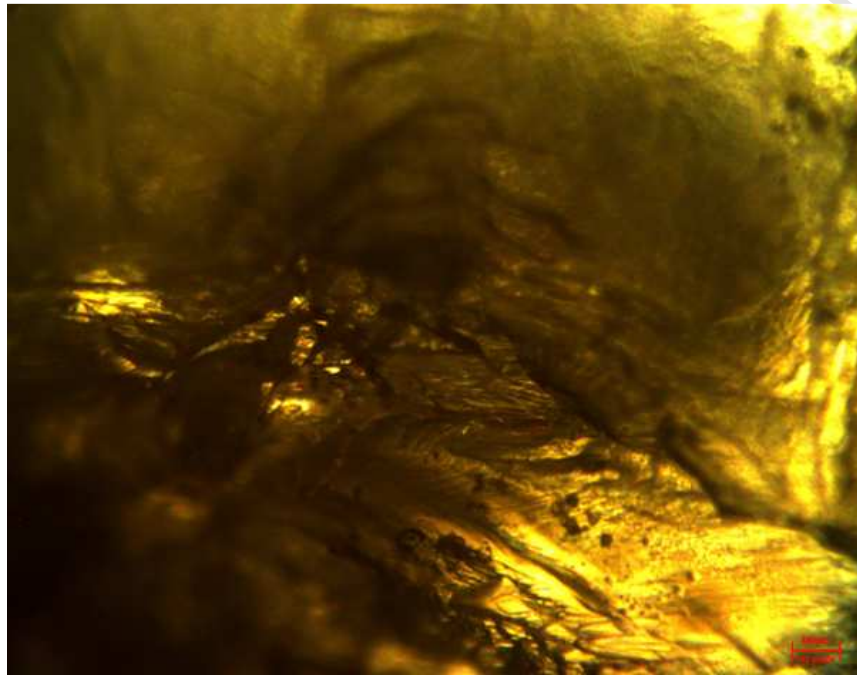


Fig. 12. Laser damage pattern of MPMN single crystal

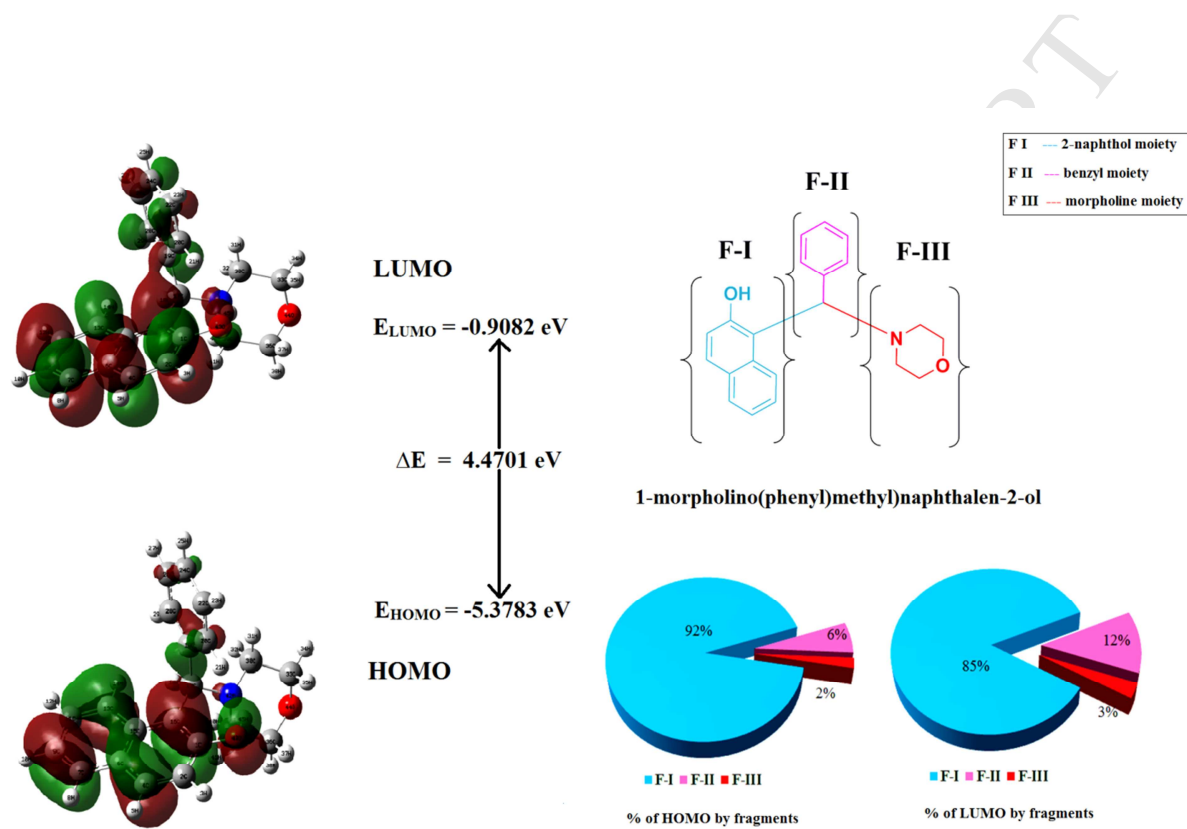


Fig. 13. HOMO and LUMO plot of MPMN

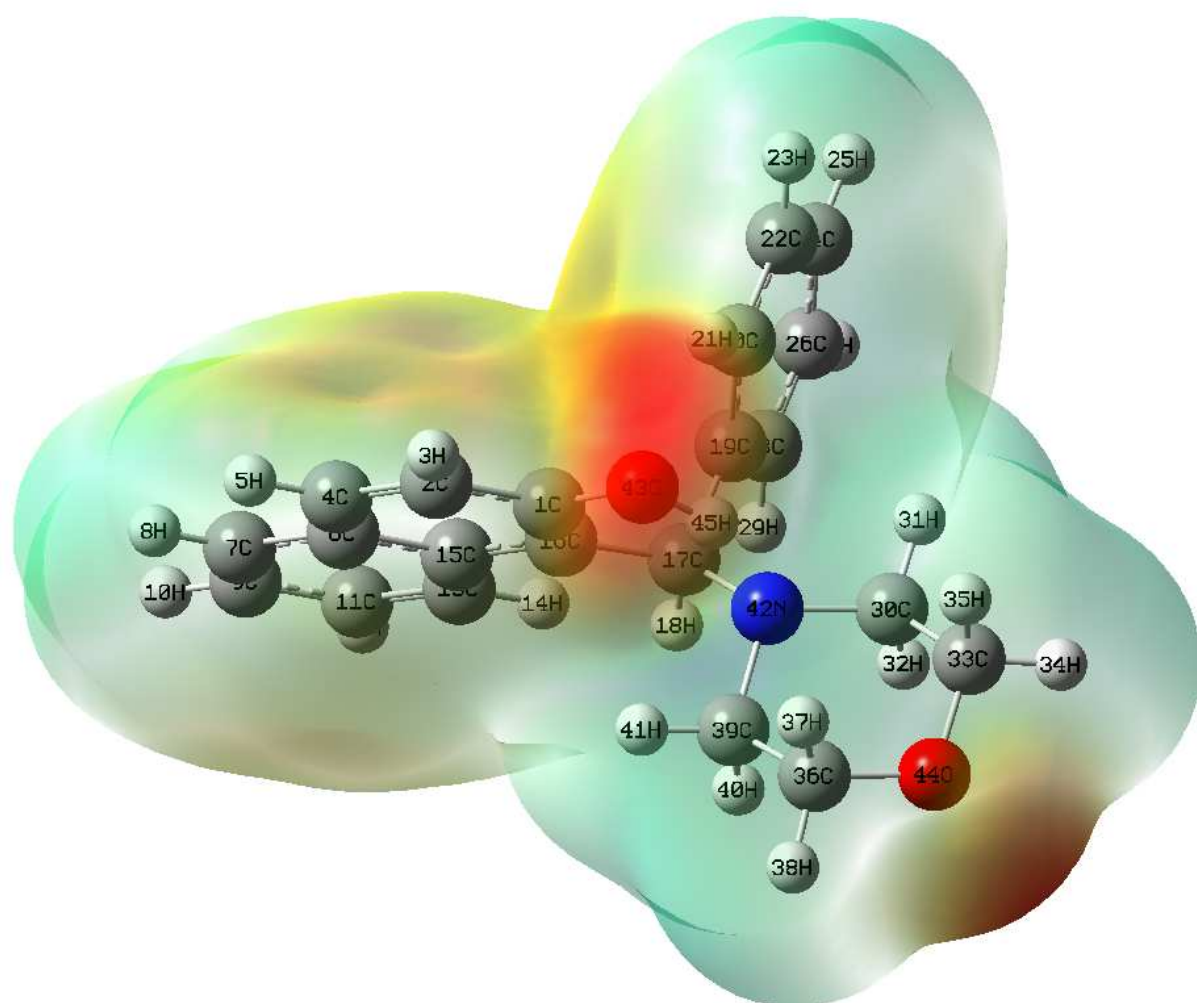


Fig. 14. Electro Static Potential Map of MPMN

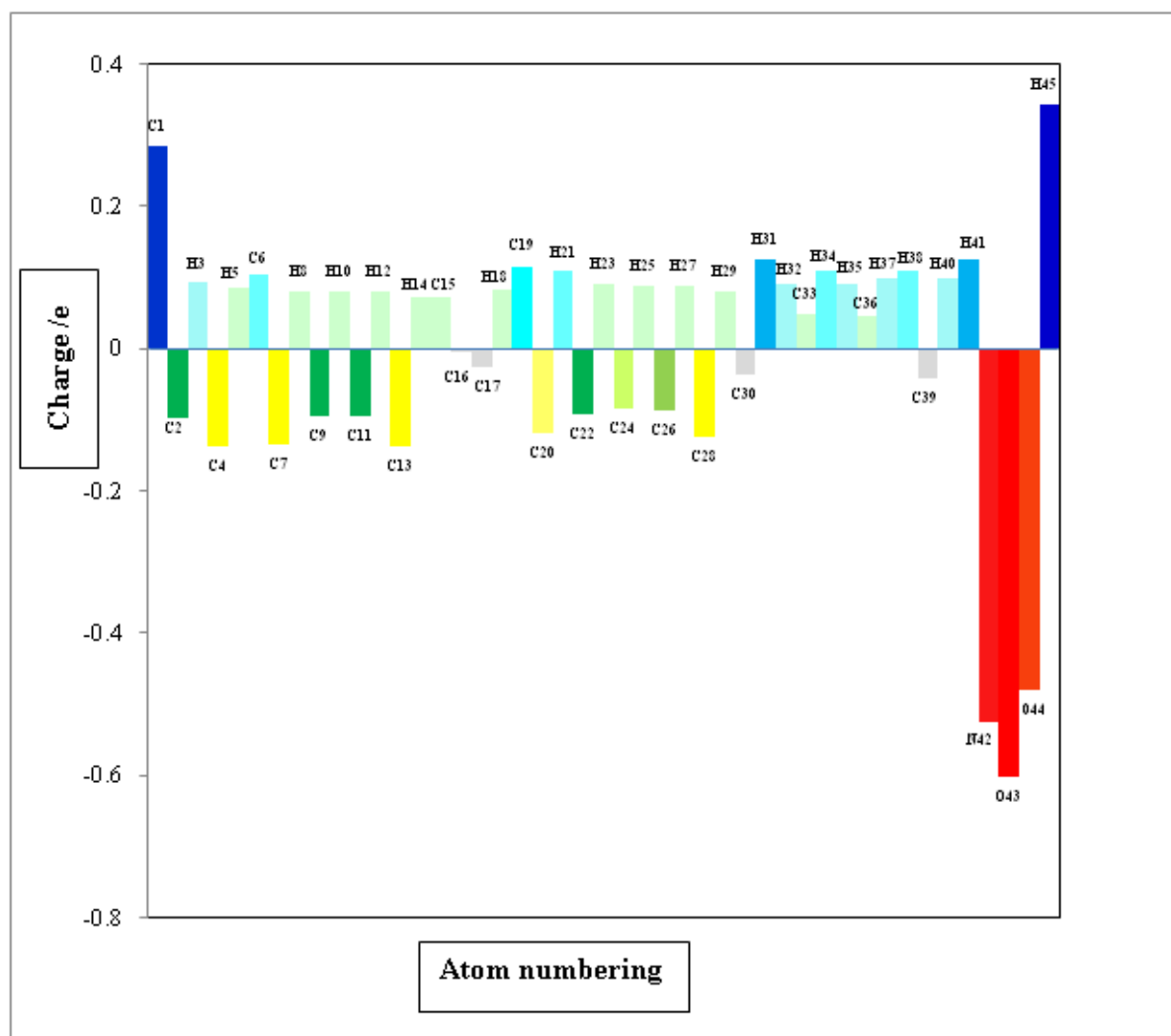


Fig. 15. Mulliken's charge distribution of MPMN

Table 1: Crystallographic data collection parameters for MPMN and its refinement

CCDC	1029398
Empirical formula	C ₂₁ H ₂₁ NO ₂
Formula weight	319.31
Temperature	293(2) K
Wavelength	0.71073 Å
Crystal system, space group	Monoclinic, Cc
Unit cell dimensions	a = 10.6592 (5) Å α = 90 °. b = 18.9868(8) Å β = 101.087 °. c = 16.7475(9) Å γ = 90 °.
Volume	3326.2 (3) Å ³
Z, Calculated density	8, 1.276 Mg/m ³
Absorption coefficient	0.082 mm ⁻¹
F (000)	1360
Crystal size	0.35 x 0.35 x 0.30 mm
Theta ranges for data collection	2.15 to 26.0 deg.
Limiting indices	-12 ≤ h ≤ 13, -23 ≤ k ≤ 23, -20 ≤ l ≤ 20
Reflections collected / unique	19670 / 6433 [R (int) = 0.0239]
Completeness to theta	= 26.0 100.0 %
Absorption correction	Semi-empirical from equivalents
Max. and min. transmission	0.9799 and 0.9710
Refinement method	Full-matrix least-squares on F ²
Data / restraints / parameters	6433 / 4 / 441
Goodness-of-fit on F ²	1.063
Final R indices [I > 2 sigma (I)]	R1 = 0.0352, wR2 = 0.0716
R indices (all data)	R1 = 0.0514, wR2 = 0.0805
Absolute structure parameter	0.3 (8)
Largest diff. peak and hole	0.128 and -0.137 e. Å ⁻³

Table 2: Hydrogen bonding geometry of MPMN [\AA and $^\circ$] from single crystal XRD

D-H...A (\AA, $^\circ$)	d(D-H)	d(H...A)	d(D...A)	\angle(DHA)
43O-45H...42N ^a	0.880(2)	1.790(3)	2.602(3)	151(3)
43O-45H...42N ^b	0.850(2)	1.800(3)	2.593(3)	153(4)
4C-5H...44O(i) ^a	0.930	2.661(2)	3.491(4)	149(2)
7C-8H...44O(i) ^a	0.930	2.777(2)	3.579(4)	145(3)
4C-5H...44O(i) ^b	0.930	2.676(2)	3.481(4)	145(2)
9C-10H...43O(ii) ^b	0.930	2.625(2)	3.471(5)	151(2)
24C-25H...44O(iii) ^b	0.930	2.758(2)	3.553(4)	143(2)

Symmetry codes: (i) $x+1/2, y-1/2, z$; (ii) $x, -y, z-1/2$; (iii) $x-1/2, y-1/2, z$

^a - Hydrogen bond interactions for **A**

^b - Hydrogen bond interactions for **B**

Table 3: Comparison between selected optimized geometrical parameters and experimental crystallographic parameters of MPMN

Bond length (Å)	Calc.	Exp.		Bond angle (°)	Calc.	Exp.	
		A	B			A	B
1C-2C	1.420	1.409 (3)	1.407 (3)	2C-1C-16C	121.18	121.32 (18)	121.57 (18)
1C1-16C	1.395	1.372 (3)	1.377 (2)	2C-1C-43O	115.64	115.42 (17)	115.33 (17)
1C-43O	1.358	1.361 (2)	1.359 (2)	16C-1C-43O	123.16	123.26 (16)	123.08 (17)
2C-4C	1.368	1.340 (3)	1.346 (3)	1C-2C-4C	120.49	120.39 (19)	120.10 (2)
4C-6C	1.420	1.401 (3)	1.404 (3)	6C-7C-9C	121.92	121.60 (2)	121.90 (2)
6C-7C	1.418	1.402 (3)	1.410 (3)	2C-4C-6C	120.85	121.21 (18)	121.14 (19)
6C-15C	1.437	1.425 (2)	1.416 (3)	22C-24C-26C	119.47	119.20 (2)	119.50 (2)
7C-9C	1.376	1.351 (3)	1.340 (4)	1C-16C-15C	118.77	118.78 (16)	118.44 (16)
9C-11C	1.412	1.401 (3)	1.392 (4)	20C-19C-28C	118.01	118.11(19)	118.01 (18)
11C-13C	1.378	1.364 (3)	1.364 (3)	17C-42N-30C	114.06	113.58 (14)	114.58 (13)
13C-15C	1.424	1.408 (3)	1.410 (3)	30C-42N-39C	108.77	107.64 (14)	107.47 (14)
15C-16C	1.436	1.422 (2)	1.420 (2)	33C-30C-42N	109.69	110.09 (17)	109.71 (16)
16C-17C	1.533	1.524 (2)	1.518 (2)	33C-44O-36C	110.51	109.51 (16)	109.54 (15)
17C-19C	1.529	1.523 (2)	1.520 (2)				
17C-42N	1.500	1.488 (2)	1.496 (2)			Exp.	
19C-20C	1.403	1.379 (3)	1.376 (3)	Torsion angle (°)	Calc.	A	B
19C-28C	1.399	1.375 (3)	1.380 (3)	16C-1C-2C-4C	-0.13	0.40 (3)	-0.20 (3)
20C-22C	1.393	1.380 (3)	1.375 (3)	43O-1C-2C-4C	179.82	-179.75 (18)	178.57 (19)
22C-24C	1.397	1.370 (3)	1.360 (3)	2C-1C-16C-15C	0.71	0.20 (3)	-0.30 (3)
24C-26C	1.393	1.372 (4)	1.378 (3)	43O-1C-16C-15C	-179.23	-179.66 (16)	-178.98 (17)
26C-28C	1.396	1.374 (3)	1.378 (3)	44O-36C-39C-42N	-58.16	-59.30 (2)	-60.80 (2)
30C-33C	1.526	1.495 (3)	1.501 (3)	11C-13C-15C-6C	-0.84	1.70 (3)	-0.80 (3)
30C-42N	1.474	1.469 (2)	1.464 (2)	22C-24C-26C-28C	-0.18	1.10 (4)	-0.20 (3)
33C-44O	1.419	1.415 (2)	1.414 (3)	42N-17C-19C-20C	-94.46	-99.30 (2)	-94.47 (19)
36C-39C	1.525	1.502 (3)	1.499 (3)	43O-1C-16C-17C	-2.22	3.40 (3)	-5.00 (3)
36C-44O	1.420	1.409 (3)	1.413 (3)	24C-26C-28C-19C	0.36	-1.70 (3)	-0.80 (3)
39C-42N	1.478	1.465 (2)	1.469 (2)	16C-17C-42N-39C	67.03	172.83 (15)	67.03 (17)

Table 4: Molecular polarizabilities and dipole moment of MPMN

Dipole moment (Debye)		Polarizability (a.u)		Hyper Polarizability (a.u)	
μ_x	0.3581	α_{xx}	253.9083	β_{xxx}	-188.3211
μ_y	1.2326	α_{yy}	14.7938	β_{yyy}	72.7952
μ_z	-1.0937	α_{zz}	215.5312	β_{zzz}	90.4603
μ	1.6863	α_{xy}	20.4715	β_{xyy}	92.9026
		α_{xz}	-29.9672	β_{xxy}	-174.1053
		α_{yz}	216.7523	β_{xxz}	58.3121
		$\Delta\alpha$	73.0372×10^{-24} esu	β_{xzz}	-6.8525
		α	23.9211×10^{-24} esu	β_{yzz}	-72.8993
				β_{yyz}	-9.7147
				β_{xyz}	-5.0893
				β	$2.1191 \times 10^{-30} \text{ cm}^5 \text{ esu}^{-1}$

Highlights

- Optically good quality bulk size organic single crystal was grown by slow evaporation technique
- The laser damage threshold was found to be 1.006 GW/cm².
- The relationship between the molecular structure and the optical properties was studied by DFT and reported for the first time.
- The results shows the suitability of the material for the electro-optic applications